

# Resonant oscillations of GeV - TeV neutrinos in internal shocks from gamma-ray burst jets inside the stars

Nissim Fraija <sup>\*</sup>

*Instituto de Astronomía, Universidad Nacional Autónoma de México, Circuito Exterior, C.U., A. Postal 70-264, 04510 México D.F., México*

18 September 2018

## ABSTRACT

High-energy neutrinos generated in collimated jets inside the progenitors of gamma-ray bursts (GRBs) have been related with the events detected by IceCube. These neutrinos, produced by hadronic interactions of Fermi-accelerated protons with thermal photons and hadrons in internal shocks, are the only signature when jet has not broken out or failed. Taking into account that the photon field is thermalized at keV energies and the standard assumption that the magnetic field maintains a steady value throughout the shock region (with a width of  $10^{10} - 10^{11}$  cm in the observed frame), we study the effect of thermal and magnetized plasma generated in internal shocks on the neutrino oscillations. We calculate the neutrino effective potential generated by this plasma, the effects of the envelope of the star, and the vacuum on the path to Earth. By considering these three effects, the two (solar, atmospheric and accelerator parameters) and three neutrino mixing, we show that although GeV - TeV neutrinos can oscillate resonantly from one flavor to another, a nonsignificant deviation of the standard flavor ratio (1:1:1) could be expected on Earth.

**Key words:** Long Gamma-ray burst: High-energy Neutrinos: – Neutrino Oscillation

## 1 INTRODUCTION

Long gamma-ray bursts (LGRBs) have been associated to core collapse of massive stars leading to supernovae (CCSNe) of type Ib,c and II. Type Ic supernovae are believed to be He stars with radius  $R_* \approx 10^{11}$  cm, and type II and Ib are thought to have a radius of  $R_* \approx 3 \times 10^{12}$  cm. Depending on the luminosities and durations, successful LGRBs have revealed a variety of GRB populations: low-luminosity (ll), ultra-long (ul) and high-luminosity (hl) GRBs (Mészáros & Waxman 2001; Liang et al. 2007; Gendre et al. 2013). While llGRBs and ulGRBs have a typical duration of ( $\sim 10^3 - 10^4$  s), hlGRBs have a duration of tens to hundreds of seconds. Another important population associated with CCSNe, although unobservables in photons, are failed GRBs which could be much more frequent than successful ones, limited only by the ratio of type Ib/c and type II SNe to GRBs rates. This population has been characterized by having high-luminosities, mildly relativistic jets and durations from several to ten seconds (Huang et al. 2002; Mészáros & Waxman 2001; Soderberg & et al. 2006, 2010). Neutrinos are useful for studying the insides of stars, especially where photons cannot be observed either because jet fails or has not broken out yet, so in this case, they could be the only signature that would display the dynamics of the star. High-energy (HE) neutrinos from this population of stars have been pointed out to contribute significantly to the extragalactic neutrino background

(ENB) (Murase & Ioka 2013; Fraija 2014a; Taboada 2010; Murase et al. 2014; Waxman 2013; Razzaque 2013; Murase et al. 2013) and to explain the recent detections of TeV- PeV neutrinos by IceCube (IceCube Collaboration et al. 2013; Aartsen et al. 2014).

Measurements of HE neutrino properties such as flavor content would be involved with new physics if a deviation of the standard flavor ratio were observed (Learned & Pakvasa 1995; Athar et al. 2000; Kashti & Waxman 2005; Mena et al. 2014). The neutrino flavor ratio is expected to be at the source,  $\phi_{\nu_e}^0 : \phi_{\nu_\mu}^0 : \phi_{\nu_\tau}^0 = 1 : 2 : 0$  and on Earth (due to neutrino oscillations between the source and Earth)  $\phi_{\nu_e}^0 : \phi_{\nu_\mu}^0 : \phi_{\nu_\tau}^0 = 1 : 1 : 1$  and  $\phi_{\nu_e}^0 : \phi_{\nu_\mu}^0 : \phi_{\nu_\tau}^0 = 1 : 1.8 : 1.8$  for neutrino energies lesser and greater than 300 TeV, respectively (Kashti & Waxman 2005). Also measurement of a non-zero  $\theta_{13}$  mixing angle coming from astrophysical sources could be relevant to clarify the neutrino mass hierarchy as well as CP violation searches in neutrino oscillations (Nunokawa et al. 2008; Bandyopadhyay & et al. 2009; Forero et al. 2012).

As known, neutrino properties are modified when they propagate in a thermal and magnetized medium. A massless neutrino acquires an effective mass and an effective potential. The resonant conversion of active neutrino from one flavor to another ( $\nu_e \leftrightarrow \nu_\mu, \nu_\tau$ ) due to thermal and magnetized medium has been explored in many astrophysical contexts and has had relevant consequences in the dynamics of them (Wolfenstein 1978a; Ruffert & Janka 1999; Goodman et al. 1987; Volkas & Wong 2000; Dasgupta et al. 2008; Erdas & Isola 2000; D’Olivo & Nieves 1996b, 1994, 1996a; D’Olivo et al. 1992; D’Olivo et al. 2003; Nötzold & Raffelt 1988; Enqvist et al.

\* E-mail: nifraija@astro.unam.mx

1991). For instance, [Fraija \(2014b\)](#) has showed that the effect of magnetic field in the dynamics of the fireball evolution of GRB was to decrease the proton-to-neutron ratio aside from the number of multi-GeV neutrinos expected in a neutrino detector.

Neutrino oscillations in vacuum and by matter effects in the failed GRB framework (along the jet and envelope of the star) have been examined by many authors ([Mena et al. 2007](#); [Razzaque & Smirnov 2010](#); [Sahu & Zhang 2010](#); [Osorio Oliveros et al. 2013](#); [Fraija 2014a](#)) and although these authors have studied the oscillations on the surface of the star due to its envelope, the effect of thermal and magnetic field plasma generated on internal shocks has not been explored. In this paper we calculate the effect of the magnetized and thermal shocked plasma on neutrino oscillations and then we estimate the flavor ratio on Earth. The organization of the paper is as follows: In section 2, we show a brief description of internal shocks. In section 3, we derive firstly, the neutrino effective potential for  $m_W \ll E_\nu$  as a function of the magnetic field, temperature, angle (between the neutrino propagation and magnetic field) and chemical potential and secondly, the neutrino effective potential produced by the envelope of the star. In section 4 we derive the resonance condition, the flip probability for two and three-neutrino mixing and the flavor ratio expected on Earth, and in section V we discuss our results. We hereafter use  $Q_x \equiv Q/10^x$  in c.g.s. units and  $\hbar=c=1$  in natural units.

## 2 DESCRIPTION OF INTERNAL SHOCKS

One of the most prosperous theory to explain the prompt emission and the afterglow in successful GRBs is the fireball model ([Zhang & Mészáros 2004](#); [Mészáros 2006](#)). A GRB is considered successful when the jet drills inside the progenitor and breaks through the stellar envelope, otherwise it is taken into account as a failed GRB. When the jet encounters the stellar envelope two shocks are involved: an outgoing, or forward, shock ([Rees & Meszaros 1994](#); [Paczynski & Rhoads 1993](#)) and another one that propagates back decelerating the ejecta, the reverse shock ([Meszaros & Rees 1994](#); [Rees & Meszaros 1994](#)). The jet dynamics is mainly dominated by the jet head, which is controlled by the ram pressure balance between the reverse and forward shock. If the luminosity ( $L_j$ ) is low enough and/or the density of the stellar envelope is high enough, then the hydrodynamic jet is collimated and internal shocks might occur inside the progenitor ([Mizuta & Ioka 2013](#); [Bromberg et al. 2011](#); [Murase & Ioka 2013](#)). In this model, inhomogeneities in the jet lead to internal shell collisions, higher shells ( $\Gamma_h$ ) catching slower shells ( $\Gamma_l$ ). The kinetic energy of ejecta is partially dissipated via these internal shocks which take place at a distance of  $r_j = 2\Gamma^2 t_\nu < R_*$ , where  $t_\nu$  is the variability time scale of the central object,  $\Gamma \simeq \sqrt{\Gamma_h \Gamma_l}$  is the bulk Lorentz factor of the propagating shock and  $R_*$  is the radius of the progenitor's stellar surface. The constraint  $r_j < R_*$  gives rise to those shocks inside the star. The physical width of the internal shock is lower by a factor of  $\Gamma$ , i.e.  $\Delta r_j = \Gamma t_\nu$ . These internal shocks are expected to be collisionless, so that particles may be accelerated. In internal shocks the total energy density  $U = 1/(8\pi m_p) \Gamma^{-4} L_j t_\nu^{-2}$  is equipartitioned to generate and/or amplify the magnetic field  $\epsilon_B = U_B/U = (B^2/8\pi)U$  ([Piran 2005](#)) and to accelerate particles  $\epsilon_e = U_e/U$ , where  $m_p$  is the proton mass. Then, the magnetic field generated at the shocks is written as

$$B' = \epsilon_B^{1/2} \Gamma^{-2} L_j^{1/2} t_\nu^{-1}. \quad (1)$$

It is important to say that the strength of the magnetic field falls out of the shocked region achieving some Gauss and although its direction might be random, it is mostly transverse to the jet direction ([Razzaque & Smirnov 2010](#)). From the causality condition, the coherence length of such magnetic field is only the order of  $\lambda_B \sim t_\nu$ . On the other hand, electrons are accelerated up to ultra-relativistic energies and then are cooled down rapidly in the presence of the magnetic field, producing the prompt emission by synchrotron radiation. The opacity to Thomson scattering is  $\tau'_{th} = \frac{\sigma_T}{4\pi m_p} \Gamma^{-3} L_j t_\nu^{-1}$  and photons thermalize at a black body temperature with peak energy given by ([Razzaque et al. 2004](#))

$$T'_\gamma \simeq \frac{1.2}{\pi} \epsilon_e^{1/4} L_j^{1/4} \Gamma^{-1} t_\nu^{-1/2}, \quad (2)$$

where  $\sigma_T$  is the Thompson cross section.

Protons are also accelerated and cooled down in internal shocks via electromagnetic (synchrotron radiation and inverse Compton (IC) scattering) and hadronic (proton-photon and proton-proton interactions) channels. Proton-photon and proton-proton interactions take place when accelerated protons interact with thermal keV photons (eq. 2) and proton density at the shock,  $n'_p = 1/(8\pi m_p) \Gamma^{-4} L_j t_\nu^{-2}$  ([Mészáros & Waxman 2001](#)). In both interactions HE charged pions and kaons are produced;  $p + \gamma/p \rightarrow X + \pi^\pm/K^\pm$ , and subsequently neutrinos  $\pi^+ \rightarrow \mu^+ + \nu_\mu \rightarrow e^+ + \nu_e + \bar{\nu}_\mu + \nu_\mu$  and  $\pi^- \rightarrow \mu^- + \bar{\nu}_\mu \rightarrow e^- + \bar{\nu}_e + \nu_\mu + \bar{\nu}_\mu$ . In this approach, the neutrino created by these processes will lie in the TeV - PeV energy range ([Murase & Ioka 2013](#); [Fraija 2014a](#); [Razzaque & Smirnov 2010](#)).

## 3 NEUTRINO EFFECTIVE POTENTIAL

In this section we are going to compute the neutrino effective potential due to the magnetized and thermal shocked plasma, and the envelope of the star.

### 3.1 Magnetized and thermal plasma

Recently, [Fraija \(2014b\)](#) derived the neutrino self-energy and effective potential up to order  $m_W^{-4}$  at strong, moderate and weak magnetic field approximation as a function of temperature, chemical potential and neutrino energy for moving neutrinos along the magnetic field. In this subsection, we will calculate the neutrino effective potential at the moderate and weak magnetic field limit for any direction of neutrino propagation. Therefore, following [Fraija \(2014b\)](#) we will show the equations that are more relevant for deducing the neutrino effective potential.

The neutrino effective potential is calculated by means of the dispersion relation

$$V_{eff} = k_0 - |\mathbf{k}|, \quad (3)$$

where  $\mathbf{k}$  is estimated through the neutrino field equation in a medium ([Nötzold & Raffelt 1988](#); [Enqvist et al. 1991](#))

$$[k - \Sigma(k)]\psi_L = 0, \quad (4)$$

and  $\sigma_l(k) = \mathcal{R}(a_\parallel k_\parallel + a_\perp k_\perp + b\mu + cb)\mathcal{L}$  is obtained from the real part of its self-energy diagram. Here  $k_\parallel^\mu = (k^0, k^3)$  and  $k_\perp^\mu = (k^1, k^2)$  are the momentum along and perpendicular to the magnetic field, respectively,  $u^\mu$  stands for the 4-velocity of the center-of-mass of the medium given by  $u^\mu = (1, \mathbf{0})$ ,  $\mathcal{R} = \frac{1}{2}(1 + \gamma_5)$

and  $\mathcal{L} = \frac{1}{2}(1 - \gamma_5)$  are the projection operators and a, b, and c are the Lorentz scalars which are functions of neutrino energy, momentum and magnetic field. These scalars are calculated from the neutrino self-energy due to CC and NC interactions of neutrino with the background particles. The effect of the magnetic field is introduced through the 4-vector  $b^\mu$  which is given by  $b^\mu = (0, \hat{\mathbf{b}})$  (Fraija 2014b). Using the Dirac algebra and from the dispersion relation (eq. 3), the neutrino effective potential can be written as

$$V_{eff} = b - c \cos \varphi - a_\perp |\mathbf{k}| \sin^2 \varphi, \quad (5)$$

where  $\varphi$  is the angle between the neutrino momentum and the magnetic field vector. Otherwise, the effective potential that is applicable to the neutrino oscillations in matter is  $V_{eff} = V_e - V_{\mu,\tau}$  which depends only on electron density (Wolfenstein 1978b; D'olivo et al. 1992). For that reason, although the one-loop neutrino self-energy comes from three parts; the W-exchange, Z-exchange and tadpole (Babaev 2004; Erdas et al. 1998; Sahu et al. 2009a,b), we will only consider the neutrino effective potential due to charged currents  $\Sigma(k) = \Sigma_W(k)$ . We will use the finite temperature field theory formalism and the Schwinger's proper time method to include the magnetic field (Schwinger 1951). From the W-exchange diagram (see fig. 1), the self-energy can be explicitly written as

$$-i\Sigma(k) = \mathcal{R} \left[ \frac{g^2}{2} \int \frac{d^4 p}{(2\pi)^4} \gamma_\mu S_\ell(p) \gamma_\nu W^{\mu\nu}(q) \right] \mathcal{L}, \quad (6)$$

where  $g^2 = 4\sqrt{2}G_F m_W^2$  is the weak coupling constant,  $W^{\mu\nu}$  is the W-boson propagator that in unitary gauge can be written as (Erdas et al. 1998; Sahu et al. 2009b)

$$W^{\mu\nu}(q) = \frac{g^{\mu\nu}}{m_W^2} \left( 1 + \frac{q^2}{m_W^2} \right) - \frac{q^\mu q^\nu}{m_W^4} + \frac{3ie}{2m_W^4} F^{\mu\nu}, \quad (7)$$

here  $m_W$  is the W-boson mass,  $G_F$  is the Fermi coupling constant,  $g^{\mu\nu}$  is the metric tensor and  $F^{\mu\nu}$  is the electromagnetic field tensor. From eq. (6),  $S_\ell(p)$  is the charged lepton propagator which is split in two propagators; one in presence of a uniform background magnetic field ( $S_\ell^0(p)$ ) and the other in a magnetized medium ( $S_\ell^\beta(p)$ ), then it can be written as

$$S_\ell(p) = S_\ell^0(p) + S_\ell^\beta(p). \quad (8)$$

We can express the charged lepton propagator in presence of a uniform background magnetic field as

$$iS_\ell^0(p) = \int_0^\infty e^{\Phi(p,s)} G(p,s) ds, \quad (9)$$

where the functions  $\Phi(p,s)$  and  $G(p,s)$  are written as

$$\begin{aligned} \Phi(p,s) &= is(p_0^2 - m_\ell^2) - is[p_3^2 + \frac{\tan z}{z} p_\perp^2], \\ G(p,s) &= \sec^2 z [\mathbf{A} + i\mathbf{B}\gamma_5 \\ &\quad + m_\ell(\cos^2 z - i\sigma_3^3 \sin z \cos z)], \end{aligned} \quad (10)$$

where  $m_\ell$  is the mass of the charged lepton,  $p_\parallel^2 = p_0^2 - p_3^2$ ,  $p_\perp^2 = p_1^2 + p_2^2$  are the projections of the momentum on the magnetic field direction and  $z = eBs$ , being  $e$  the magnitude of the electron charge. Additionally, the covariant vectors are given as follows,  $A_\mu = p_\mu - \sin^2 z(p \cdot u u_\mu - p \cdot b b_\mu)$ ,  $B_\mu = \sin z \cos z(p \cdot u b_\mu - p \cdot b u_\mu)$ , and  $\sigma_3^3 = \gamma_5 \mathbf{b} \cdot \mathbf{u}$ . The other term in eq. (8) (due to magnetized medium) is given by (D'Olivo & Nieves 1996a)

$$S_\ell^\beta(p) = i\eta_F(p \cdot u) \int_{-\infty}^\infty e^{\Phi(p,s)} G(p,s) ds, \quad (11)$$

where  $\eta_F(p \cdot u)$  contains the distribution functions of the particles in the medium which are given by:

$$\eta_F(p \cdot u) = \frac{\theta(p \cdot u)}{e^{\beta(p \cdot u - \mu_\ell)} + 1} + \frac{\theta(-p \cdot u)}{e^{-\beta(p \cdot u - \mu_\ell)} + 1}, \quad (12)$$

where  $\beta$  and  $\mu_\ell$  are the inverse of the medium temperature and the chemical potential of the charged lepton. By evaluating eq. (6) explicitly we obtain

$$Re\Sigma(k) = \mathcal{R} [a_\perp k_\perp + b\mathbf{u} + cb] \mathcal{L}, \quad (13)$$

where the Lorentz scalars are given by (Fraija 2014b)

$$\begin{aligned} a_\perp &= -\frac{\sqrt{2}G_F}{m_W^2} \left\{ E_{\nu_e} (n_e - \bar{n}_e) + k_3 (n_e^0 - \bar{n}_e^0) \right\} \\ &\quad + \frac{eB}{2\pi^2} \int_0^\infty dp_3 \sum_{n=0}^\infty (2 - \delta_{n,0}) \left( \frac{m_e^2}{E_n} - \frac{H}{E_n} \right) (f_{e,n} + \bar{f}_{e,n}), \quad (14) \\ b &= \sqrt{2}G_F \left[ \left( 1 + \frac{E_{\nu_e}^2}{m_W^2} \right) (n_e - \bar{n}_e) + \frac{E_{\nu_e} k_3}{m_W^2} (n_e^0 - \bar{n}_e^0) \right. \\ &\quad \left. - \frac{eB}{\pi^2 m_W^2} \int_0^\infty dp_3 \sum_{n=0}^\infty (2 - \delta_{n,0}) E_{\nu_e} \left\{ E_n \delta_{n,0} + \left( E_n - \frac{m_e^2}{2E_n} \right) \right\} (f_{e,n} + \bar{f}_{e,n}) \right], \quad (15) \end{aligned}$$

and

$$\begin{aligned} c &= \sqrt{2}G_F \left[ \left( 1 - \frac{k_3^2}{m_W^2} \right) (n_e^0 - \bar{n}_e^0) - \frac{E_{\nu_e}^2}{m_W^2} (n_e - \bar{n}_e) \right. \\ &\quad \left. - \frac{eB}{\pi^2 m_W^2} \int_0^\infty dp_3 \sum_{n=0}^\infty (2 - \delta_{n,0}) E_{\nu_e} \left\{ \left( E_n - \frac{m_e^2}{E_n} \right) \delta_{n,0} \right. \right. \\ &\quad \left. \left. + \left( E_n - \frac{3}{2} \frac{m_e^2}{E_n} - \frac{H}{E_n} \right) \right\} (f_{e,n} + \bar{f}_{e,n}) \right]. \quad (16) \end{aligned}$$

Here the electron number density and electron distribution function are

$$n_e(\mu, T, B) = \frac{eB}{2\pi^2} \sum_{n=0}^\infty (2 - \delta_{n,0}) \int_0^\infty \frac{dp_3}{e^{\beta(E_{e,n} - \mu)} + 1}, \quad (17)$$

and

$$f(E_{e,n}, \mu) = \frac{1}{e^{\beta(E_{e,n} - \mu)} + 1}, \quad (18)$$

respectively, with  $\bar{f}_{e,n}(\mu, T) = f_{e,n}(-\mu, T)$  and  $E_{e,n} = \sqrt{p_3^2 + m_e^2} + H$  with  $H = 2neB$ . Solving the integral terms in eqs. (14), (15) and (16) and replacing them in eq. (5) we calculate the neutrino effective potential for two cases: the moderate and the weak magnetic field limit.

### 3.1.1 Moderate Magnetic field limit

In the moderate field approximation ( $B/B_c \leq 1$ ), the Landau levels are discrete and can be described by sums ( $\sum_n$  with  $n=1, 2, 3 \dots$ ). In this regime, the neutrino effective potential is written as

$$\begin{aligned} V_{eff, is(m)} &= \frac{\sqrt{2}G_F m_e^3 B}{\pi^2 B_c} \left[ \sum_{l=0}^\infty (-1)^l \sinh \alpha_l [F_m - G_m \cos \varphi] \right. \\ &\quad \left. - 4 \frac{m_e^2}{m_W^2} \frac{E_\nu}{m_e} \sum_{l=0}^\infty (-1)^l \cosh \alpha_l [J_m - H_m \cos \varphi] \right] \quad (19) \end{aligned}$$

where  $\alpha_l = \beta\mu(l+1)$  and the functions  $F_m, G_m, J_m, H_m$  are written in the appendix A. It is worth noting that as the magnetic field decreases the effective potential will depend less on the Landau levels.

### 3.1.2 Weak Magnetic field limit

In the weak field approximation ( $B/B_c \ll 1$ ), all levels are full and overlap each other. In this regimen, sums over the Landau levels can be described and approximated by an integral  $\sum_n \rightarrow \int dn$ , then the effective potential does not depend on the Landau levels. The potential in this regimen can be written as

$$V_{eff, is(w)} = \frac{\sqrt{2} G_F m_e^3 B}{\pi^2 B_c} \left[ \sum_{l=0}^{\infty} (-1)^l \sinh \alpha_l [F_w - G_w \cos \varphi] - 4 \frac{m_e^2}{m_W^2} \frac{E_\nu}{m_e} \sum_{l=0}^{\infty} (-1)^l \cosh \alpha_l [J_w - H_w \cos \varphi] \right] \quad (20)$$

where the functions  $F_w, G_w, J_w, H_w$  are shown in the appendix A.

## 3.2 Density profiles of envelopes

Models of density distributions in CCSNe have been widely explored (Bethe & Pizzochero 1990; Chevalier & Soker 1989; Woosley et al. 1993; Shigeyama & Nomoto 1990). We will use two models with density profiles  $\rho \propto r^{-3}$  and  $\rho \propto r^{-17/7}$ . Explicitly, the first model corresponds to a polytropic hydrogen envelope

$$\rho_1(r) = 4.0 \times 10^{-6} \left( \frac{R_\star}{r} - 1 \right)^3 \text{ g cm}^{-3}, \quad (21)$$

and the second model is a power-law fit with an effective polytropic index  $n_{eff} = 17/7$  as done for SN 1987A (Chevalier & Soker 1989)

$$\rho_2(r) = 3.4 \times 10^{-5} \text{ g cm}^{-3} \times \begin{cases} (R_\star/r)^{17/7}; & 10^{10.8} \text{ cm} < r < r_b = 10^{12} \text{ cm} \\ (R_\star/r_b)^{17/7} (r - R_\star)^5 / (r_b - R_\star)^5; & r > r_b. \end{cases} \quad (22)$$

In both cases, from the number density of electrons  $N_e = N_a \rho(r) Y_e$ , the neutrino effective potential can be written as

$$V_{eff, ss} = \sqrt{2} G_F N_e, \quad (23)$$

where  $N_a = 6.022 \times 10^{23} \text{ g}^{-1}$  is the Avogadro's number,  $Y_e = 0.5$  is the number of electrons associated per nucleon and  $\rho(r)$  is given by eqs. (21) and (22).

## 4 NEUTRINO RESONANT OSCILLATIONS

When neutrino oscillations take place in matter, a resonance could occur that would dramatically enhance the flavor mixing and could lead to a maximal conversion from one neutrino flavor to another. This resonance depends on the effective potential and neutrino oscillation parameters. The equation that determines the neutrino evolution in matter in the two and three-flavor framework is (Fraija et al. 2014)

$$U \cdot \frac{1}{2E_\nu} \mathbf{M} \cdot U^\dagger + \text{diag}(V_{eff, k}, \vec{0}), \quad (24)$$

where

$$\mathbf{M} = \begin{cases} (-\delta m^2, 0) & \text{for two flavors,} \\ (-\delta m_{21}^2, 0, \delta m_{32}^2) & \text{for three flavors,} \end{cases} \quad (25)$$

$\delta m_{ij}^2$  is the mass difference (Giunti & Chung 2007),  $U$  is the two- and three-neutrino mixing matrix (see appendix B, eq. B9),  $V_{eff, k}$  is the neutrino effective potentials calculated in section 3 (for  $k=is$  and  $ss$ ) and  $E_\nu$  is the neutrino energy. We hereafter use the first and second line for two- and three-neutrino mixing, respectively, as written in eq. (25). From the conversion probabilities, we obtain that the oscillation lengths are

$$L_{res} = 4\pi E_\nu \begin{cases} \frac{1}{\sqrt{(2E_\nu V_{eff, k} - \delta m^2 \cos 2\theta)^2 + (\delta m^2 \sin 2\theta)^2}}, \\ \frac{1}{\sqrt{(2E_\nu V_{eff, k} - \delta m_{32}^2 \cos 2\theta_{13})^2 + (\delta m_{32}^2 \sin 2\theta_{13})^2}}, \end{cases} \quad (26)$$

with the resonance conditions

$$2 \times 10^6 E_\nu V_{eff, k} = \begin{cases} \delta m^2 \cos 2\theta, \\ \delta m_{32}^2 \cos 2\theta_{13}. \end{cases} \quad (27)$$

In addition to the resonance condition, the dynamics of the transition from one flavor to another must be determined by adiabatic conversion through the adiabaticity parameter (Mohapatra & Pal 2004)

$$\gamma \equiv \frac{1}{2E_\nu} \left| \frac{1}{V_{eff, k}} \frac{dV_{eff, k}}{dr} \right|_r \begin{cases} \delta m^2 \sin 2\theta \tan 2\theta, \\ \delta m_{32}^2 \sin 2\theta_{13} \tan 2\theta_{13}, \end{cases} \quad (28)$$

with  $\gamma \gg 1$  or the flip probability given by

$$P_f = e^{-\pi/2 \gamma}. \quad (29)$$

By considering that the flux ratio of  $\dot{N}_{\nu_\mu} \simeq \dot{N}_{\bar{\nu}_\mu} \simeq 2\dot{N}_{\nu_e} \simeq 2\dot{N}_{\bar{\nu}_e}$  is created in the internal shocks, neutrinos firstly oscillate in matter due to the magnetized and thermal plasma and secondly oscillate to the star envelope. In vacuum, after neutrinos have left the star, they start oscillating to the Earth. Hence, from these three effects: internal shocks, envelope of the star and vacuum, the flavor ratio expected on Earth will be

$$\begin{pmatrix} \nu_e \\ \nu_\mu \\ \nu_\tau \end{pmatrix}_{Earth} = \begin{pmatrix} P_{11}^* & P_{12}^* & P_{13}^* \\ P_{21}^* & P_{22}^* & P_{23}^* \\ P_{31}^* & P_{32}^* & P_{33}^* \end{pmatrix} \begin{pmatrix} 1 \\ 2 \\ 0 \end{pmatrix}_c, \quad (30)$$

where the probabilities  $P_{ij}^*$  are derived in appendix B.

The best fit values of the two neutrino mixing are: **Solar Neutrinos:**  $\delta m^2 = (5.6_{-1.4}^{+1.9}) \times 10^{-5} \text{ eV}^2$  and  $\tan^2 \theta = 0.427_{-0.029}^{+0.033}$  (Aharmim & et al. 2011), **Atmospheric Neutrinos:**  $\delta m^2 = (2.1_{-0.4}^{+0.9}) \times 10^{-3} \text{ eV}^2$  and  $\sin^2 2\theta = 1.0_{-0.07}^{+0.00}$  (Abe & et al. 2011) and **Accelerator Neutrinos:**  $\delta m^2 = 0.5 \text{ eV}^2$  and  $\sin^2 \theta = 0.0049$  (Zeitnitz 1994; Athanassopoulos & et al. 1996, 1998). Combining solar, atmospheric, reactor and accelerator parameters, the best fit values of the three neutrino mixing are, for  $\sin^2_{13} < 0.053$ :  $\Delta m_{21}^2 = (7.41_{-0.19}^{+0.21}) \times 10^{-5} \text{ eV}^2$  and  $\tan^2 \theta_{12} = 0.446_{-0.029}^{+0.030}$  and, for  $\sin^2_{13} < 0.04$ :  $\Delta m_{23}^2 = (2.1_{-0.2}^{+0.5}) \times 10^{-3} \text{ eV}^2$  and  $\sin^2 \theta_{23} = 0.50_{-0.093}^{+0.083}$  (Aharmim & et al. 2011; Wendell & et al. 2010).

## 5 RESULTS AND CONCLUSIONS

In this analysis we have considered HE neutrinos created in the energy range of  $100 \text{ GeV} \leq E_\nu \leq 100 \text{ TeV}$  (Murase & Ioka 2013; Fraija 2014a; Razzaque & Smirnov 2010) and also we have assumed (in the CCSNe-GRB connection) progenitors such as Wolf-Rayet (WR) and blue supergiant (BSG) stars with radii  $R_\star = 10^{11} \text{ cm}$  and  $R_\star = 3 \times 10^{12} \text{ cm}$ , respectively, with formation of jets leading to internal shocks inside of them.

In internal shocks, energy is equipartitioned to generate and/or amplify the magnetic field and to accelerate particles. Electrons

and protons are expected to be accelerated in these shocks, and after to be cooled down by synchrotron radiation, inverse Compton and hadronic processes ( $p\gamma$  and  $p$ -hadron interactions). Photons produced by electron synchrotron radiation are thermalized at keV energies and serve as targets for production of HE neutrinos through  $K^\pm$ ,  $\pi^\pm$  and  $\mu^\pm$  decay products in the proton- $\gamma$  and proton-hadrons interactions. Therefore, this plasma is endowed with a magnetic field and made of protons, mesons, electrons, positrons, photons and neutrinos.

First of all, we consider those internal shocks that take place inside progenitors ( $r_j < R_*$ ), as plotted in fig. 2. In this figure, we show the contour lines of bulk Lorentz factors and variability time scales for different internal shock radii. In these plots we observe that for a typical value of variability in the range of  $10^{-3} \text{ s} \leq t_\nu \leq 1 \text{ s}$ , the values of bulk Lorentz factors are  $\Gamma \leq 34$  for a WR (left-hand figure) and  $\Gamma \leq 163$  for a BSG (right-hand figure). Taking into account internal shocks at  $r_j = 10^{10.8} \text{ cm}$  (left-hand figure) and  $r_j = 10^{12.2} \text{ cm}$  (right-hand figure) we can see that the physical width of the internal shocks is restricted to  $\Delta r_j \leq 1.8 \times 10^{10} \text{ cm}$  and  $\Delta r_j \leq 2.5 \times 10^{11} \text{ cm}$ , respectively. Once obtained the values of  $\Gamma$  and  $t_\nu$  for internal shocks inside the progenitor we compute the range of values associated to the magnetic field and temperature of the plasma, as shown in figs. 3 and 4, respectively. We plot the contour lines of the magnetic fields (fig. 3) and thermalized photons (fig. 4) for values of luminosity in the range  $10^{46} \text{ erg/s} \leq L_\gamma \leq 10^{52} \text{ erg/s}$ . Colors in light- and dark-gray backgrounds represent the regions of a WR and a BSG, respectively.

In figs. 3 and 4 one can see that the values of magnetic field and thermalized photons lie in the ranges  $10^6 \text{ G} \leq B \leq 10^{11} \text{ G}$  and  $0.1 \text{ keV} \leq T \leq 30 \text{ keV}$ , respectively. It is important to clarify that the magnetic field amplified in the internal shocks falls out of them to the magnetic field endowed by the progenitor (black hole (BH) or magnetar) (Razzaque & Smirnov 2010).

Following Fraija (2014b) and taking into account that the range of neutrino energy considered is larger than the W-boson mass ( $E_\nu \geq m_W^2$ ), we have obtained the neutrino effective potential up to an order  $m_W^{-4}$  in the moderate below  $B/B_c \sim 10^{-5}$  and weak  $B/B_c \sim 10^{-13}$  regime as a function of the observable quantities in the internal shocks: thermalized photons, magnetic field, neutrino energy and angle between the direction of neutrino propagation and the magnetic field. We plot the neutrino effective potential in both limits (moderate and weak field limits) as shown in fig. 5. The neutrino effective potential at moderate limit (figures above) and weak limit (figures below) are plotted for a magnetic field in the range of  $10^{-6} B_c < B < 10^{-4} B_c$  and  $10^{-13} B_c < B < 10^{-12} B_c$ , respectively. In both cases, we use the values of temperature  $T = (20, 24, 27 \text{ and } 30) \text{ keV}$ , angle  $\varphi = (0^\circ, 30^\circ, 60^\circ \text{ and } 90^\circ)$  and the neutrino energy  $E_\nu = 10 \text{ TeV}$ . The neutrino effective potential at the weak limit is smaller than at the moderate limit. It is worth mentioning that in the range of the magnetic field considered, the contribution of Landau levels to the effective potential at the moderate-field limit is not significant due to  $\sum_{n=1}^{\infty} \lambda_n K_i(\sigma_l \lambda_n) \sim 0$  for  $\lambda_n = \sqrt{1 + 2n B/B_c}$  and  $\sigma_l = \beta m_e (l + 1)$ . From these plots one can observe that the neutrino effective potential is positive, therefore due to its positivity ( $V_{eff, is(k)} > 0$ ) for  $k = m$  and  $w$ , neutrinos can oscillate resonantly. From the resonance condition (eq. 27) and the neutrino effective potential at moderate (eq. 19) and weak (eq. 20) limit, we plot the contour lines of temperature and chemical potential as a function of neutrino energy for which the resonance condition is satisfied, as shown in figs. 6 and 7, respectively. From these figures, one can

Energy (TeV)	$l_{res}$ (cm)			
	Solar	Atmosph.	Accelerat.	Three flav.
$10^{-2}$	$4.8 \times 10^{10}$	$1.2 \times 10^9$	$7.1 \times 10^7$	$2.6 \times 10^9$
0.5	$2.4 \times 10^{12}$	$5.9 \times 10^{10}$	$3.6 \times 10^9$	$1.3 \times 10^{11}$
10	$4.8 \times 10^{13}$	$1.2 \times 10^{12}$	$7.1 \times 10^{10}$	$2.6 \times 10^{12}$
$10^2$	$4.8 \times 10^{14}$	$1.2 \times 10^{13}$	$7.1 \times 10^{11}$	$2.6 \times 10^{13}$

**Table 1.** Resonance lengths of HE neutrinos for the best fit parameters of the two- and three-neutrino mixing.

see that temperature is a decreasing function of chemical potential and neutrino energy. As neutrino energy increases, temperature decreases steadily. Considering the values of neutrino energy ( $E_\nu = 100 \text{ GeV}, 500 \text{ GeV}, 10 \text{ TeV}$  and  $100 \text{ TeV}$ ) and  $\varphi = 90^\circ$ , we see that the temperature and chemical potential are in the range  $10 \text{ keV}$  to  $\sim 100 \text{ keV}$  and  $60 \text{ eV}$  to  $50 \text{ keV}$ , respectively. For instance, taking into account a neutrino energy of  $10 \text{ TeV}$ , from fig. 6 we can see that temperature lies in the range  $22.2$  to  $15.3 \text{ keV}$  for solar,  $23.4$  to  $16.2 \text{ keV}$  for atmospheric,  $40$  to  $26.4 \text{ keV}$  for accelerator and  $28.3$  to  $15.4 \text{ keV}$  for three-neutrino parameters, and as shown in fig. 7, temperature lies in the range  $18.3$  to  $14.1 \text{ keV}$  for solar,  $19.8$  to  $15.1 \text{ keV}$  for atmospheric,  $32.1$  to  $21.9 \text{ keV}$  for accelerator and  $24.5$  to  $18.3 \text{ keV}$  for three-neutrino parameters. In addition, we have obtained the resonance lengths which are shown in table 1. As shown in this table, the resonance lengths lie in the range  $l_{res} \sim (10^{10} \text{ to } 10^{13}) \text{ cm}$ , hence depending on the progenitor associated and the oscillation parameters, neutrinos would leave the internal shock region in different flavors of 1:2:0. For instance, taking into account the parameters of three-neutrino mixing, neutrinos with energy less than  $0.5$  ( $10$ )  $\text{TeV}$  will oscillate resonantly with a resonance length equal or less than the radius of the progenitor, either a WR or BSG. Considering parameters of accelerator experiments, neutrino energy around  $100 \text{ TeV}$  will oscillate in a BSG star before leaving it.

As the dynamics of resonant transitions is not only determined by the resonance condition, but also by adiabatic conversion, we analyze the flip probability (eq. 29) to find the regions for which neutrinos can oscillate resonantly. First of all we derive the neutrino effective potential as the function of magnetic field  $dV_{eff}/dr = \partial V_{eff}/\partial B \times \partial B/\partial r$ , and assume that at internal shocks ( $10^{10.8} \text{ cm}$  for WR and  $10^{12} \text{ cm}$  for BSGs), magnetic fields change a 10% of any variation around the radius shock scale. For instance, for a WR star,  $\partial B/\partial r = 0.1 \times 10^{-4} B_c / 10^{10.8} \text{ cm} = 6.99 \times 10^{-3} \text{ Gauss/cm}$ . We plot the flip probability as a function of neutrino energy for two and three flavors (fig 8). We divide each plot of flip probability in three regions in order to analyze the whole range of probabilities: less than  $0.2$  ( $P_\gamma \leq 0.2$ , a pure adiabatic conversion), between  $0.2$  and  $0.8$  ( $0.2 < P_\gamma < 0.8$  represents the transition region) and greater than  $0.8$  ( $P_\gamma \geq 0.8$  is a strong violation of adiabaticity) (Dighe & Smirnov 2000). In fig. 8, we use two flavors: solar (left-hand figure above), atmospheric (right-hand figure above), accelerator (left-hand figure below) and three flavor (right-hand figure below). When we use solar parameters, a pure adiabatic conversion occurs in a WR (BSG) star for neutrino energies of less than  $10^{10.5}$  ( $10^{11.7}$ )  $\text{eV}$  and  $10^{11.5}$  ( $10^{12.75}$ )  $\text{eV}$  which are endowed with  $B = 10^{-4} B_c$  and  $B = 10^{-13} B_c$ , respectively. Considering atmospheric parameters, only a pure adiabatic conversion takes place in a WR (BSG) star for neutrino energies less than  $10^{13.6}$  ( $10^{14.8}$ )  $\text{eV}$  and  $10^{14.5}$  ( $> 10^{15}$ )  $\text{eV}$  which are endowed with  $B = 10^{-4} B_c$  and  $B = 10^{-13} B_c$ , respectively. Taking

into account accelerator parameters, a pure adiabatic conversion happens in a WR (BSG) star for neutrino energies of less than  $10^{11.8}$  ( $10^{13.1}$ ) eV and  $10^{12.7} > 10^{15}$  eV with  $B = 10^{-4}B_c$  and  $B = 10^{-13}B_c$ , respectively and once again considering three neutrino mixing, a pure adiabatic conversion occurs in a WR (BSG) star for neutrino energy of less than  $10^{11.1}$  ( $10^{12.5}$ ) eV and  $10^{12.1}$  ( $10^{3.5}$ ) eV with  $B = 10^{-4}B_c$  and  $B = 10^{-13}B_c$ , respectively. Higher energies to those considered are found in regions of transition and/or those prohibited.

In addition, we have studied the HE neutrino oscillations from the neutrino effective potential generated in the star envelope (eq. 23), as shown in fig. 9. From the resonance condition (eq. 27), we obtain the contour plots of radius as a function of neutrino energy. One can see that for neutrino energy in the range  $100 \text{ GeV} < E_\nu < 100 \text{ TeV}$  the radius lies in the range  $10^{10.8} \text{ cm} < r < 10^{12.5} \text{ cm}$ . The flip probability for neutrino oscillations in the envelope of a star was studied by Fraija (2014a). The author has plotted this probability as a function of neutrino energy for density profiles [A] (eq. 21) and [B] (eq. 22) and neutrino oscillation parameters. From this analysis, Fraija (2014a) showed that neutrinos can oscillate depending on their energy and the parameters of neutrino experiments, obtaining that neutrino with energies above dozens of TeV can hardly oscillate.

Finally, considering a flux ratio  $\dot{N}_{\nu_\mu} \simeq \dot{N}_{\bar{\nu}_\mu} \simeq 2\dot{N}_{\nu_e} \simeq 2\dot{N}_{\bar{\nu}_e}$ , we estimate the neutrino flavor ratio coming from the surface of a WR and BSG to Earth, as shown in fig. 10. In this estimation, we take into account the contribution of thermal and magnetized plasma at moderate and weak  $B$  limit generated by internal shocks; at  $10^{10.8} \text{ cm}$  (second panel),  $10^{11} \text{ cm}$  (upper panel),  $10^{12} \text{ cm}$  (bottom panel) and  $10^{12.3} \text{ cm}$  (third panel), the effective potential due to the envelope of star and oscillation neutrinos in vacuum, due to the path up to Earth. In this figure we take into account two values of  $\theta_{13}$  mixing angle,  $2^\circ$  (left column) and  $11^\circ$  (right column). As shown, one can observe that a nonsignificant deviation of the standard ratio ( $\phi_{\nu_e}/\phi_{\nu_\mu}:\phi_{\nu_\mu}/\phi_{\nu_\tau}:\phi_{\nu_\tau}/\phi_{\nu_e}$ ; 1:1:1) is expected, less than 10 % for  $\theta_{13} = 11^\circ$  and only 2 % for  $\theta_{13} = 2^\circ$ . In addition, we plot the neutrino flavor ratio expected on Earth as a function of neutrino energy when the magnetic field is oriented to different angles  $0^\circ \leq \varphi \leq 75^\circ$  concerning neutrino direction, as shown in figs. 11 and 12. In fig. 11 we consider the neutrino effective potential at the moderate-field limit and internal shocks at  $r_j = 10^{12} \text{ cm}$  with a physical width  $\Delta r_j = 2 \times 10^{11} \text{ cm}$  and in fig. 12, we consider the neutrino effective potential at the weak-field limit and internal shocks at  $r_j = 10^{10.8} \text{ cm}$  with a physical width  $\Delta r_j = 1.5 \times 10^{10} \text{ cm}$ . From both plots, we can see that although the neutrino flavor ratio changes at different angles, distances of internal shocks, strength of magnetic field (moderate and weak limit) and neutrino energy in the range  $10^{11} \text{ eV} \leq E_\nu \leq 10^{14} \text{ eV}$ , this flavor ratio expected on Earth lies between 0.98 and 1.02, hence we can conclude that the directionality of magnetic fields does not affect our results. Although currently neutrino oscillations can hardly be detected, new techniques in the near future will allow us to perceive these oscillations and put limits on the neutrino mixing angles. Finally, it is worth noting that the estimated values of the bulk Lorentz factor, in particular those relying on variability time measurements, are only raw approximations, and variations by a factor of a few cannot be ruled out by existing data.

## ACKNOWLEDGEMENTS

We are thankful to the anonymous referee for a critical reading of the paper and valuable suggestions that helped improve the quality and clarity of this work. We also thank A. M. Sodelberg, J. Nieves, B. Zhang, K. Murase, W. H. Lee, F. de Colle, E. Moreno and A. Marinelli for useful discussions. NF gratefully acknowledges a Luc Binette-Fundación UNAM postdoctoral fellowship. This work was supported by the projects IG100414 and Conacyt 101958.

## REFERENCES

- Aartsen M. G., Ackermann M., Adams J., Aguilar J. A., Ahlers M., Ahrens M., Altmann D., Anderson T., Argüelles C., Arlen T. C., et al. 2014, ArXiv e-prints
- Abe K., et al. 2011, Physical Review Letters, 107, 241801
- Aharmim B., et al. 2011, ArXiv e-prints
- Akhmedov E. K., Johansson R., Lindner M., Ohlsson T., Schwetz T., 2004, Journal of High Energy Physics, 4, 78
- Athanassopoulos C., et al. 1996, Physical Review Letters, 77, 3082
- Athanassopoulos C., et al. 1998, Physical Review Letters, 81, 1774
- Athar H., Jezabek M., Yasuda O., 2000, Phys. Rev. D, 62, 103007
- Babaev E., 2004, Phys. Rev. D, 70, 043001
- Bahcall J. N., 1989, Neutrino astrophysics
- Bandyopadhyay A., et al. 2009, Reports on Progress in Physics, 72, 106201
- Bethe H. A., Pizzochero P., 1990, ApJ, 350, L33
- Bromberg O., Nakar E., Piran T., Sari R., 2011, ApJ, 740, 100
- Chevalier R. A., Soker N., 1989, ApJ, 341, 867
- Dasgupta B., Dighe A., Mirizzi A., Raffelt G., 2008, Phys. Rev. D, 78, 033014
- Dighe A. S., Smirnov A. Y., 2000, Phys. Rev. D, 62, 033007
- D’Olivo J. C., Nieves J., 1994, Nuclear Physics B Proceedings Supplements, 35, 466
- D’Olivo J. C., Nieves J. F., 1996a, Physics Letters B, 383, 87
- D’Olivo J. C., Nieves J. F., 1996b, International Journal of Modern Physics A, 11, 141
- D’Olivo J. C., Nieves J. F., Sahu S., 2003, Phys. Rev. D, 67, 025018
- D’olivo J. C., Nieves J. F., Torres M., 1992, Phys. Rev. D, 46, 1172
- Enqvist K., Kainulainen K., Maalampi J., 1991, Nuclear Physics B, 349, 754
- Erdas A., Isola C., 2000, Physics Letters B, 494, 262
- Erdas A., Kim C. W., Lee T. H., 1998, Phys. Rev. D, 58, 085016
- Forero D. V., Tórtola M., Valle J. W. F., 2012, Phys. Rev. D, 86, 073012
- Fraija N., 2014a, MNRAS, 437, 2187
- Fraija N., 2014b, ApJ, 787, 140
- Fraija N., Bernal C. G., Hidalgo-Gaméz A. M., 2014, MNRAS, 442, 239
- Gendre B., Stratta G., Atteia J. L., Basa S., Bor M., Coward D. M., Cutini S., D’Elia V., Howell E. J., Klotz A., Piro L., 2013, The Astrophysical Journal, 766, 30
- Giunti C., Chung W. K., 2007, Fundamentals of Neutrino Physics and Astrophysics. Oxford University Press
- Gonzalez-Garcia M. C., 2011, Physics of Particles and Nuclei, 42, 577
- Gonzalez-Garcia M. C., Maltoni M., 2008, Phys. Rep., 460, 1
- Gonzalez-Garcia M. C., Nir Y., 2003, Reviews of Modern Physics, 75, 345

Goodman J., Dar A., Nussinov S., 1987, ApJ, 314, L7  
 Huang Y. F., Dai Z. G., Lu T., 2002, MNRAS, 332, 735  
 IceCube Collaboration Aartsen M. G., Abbasi R., Abdou Y., Ackermann M., Adams J., Aguilar J. A., Ahlers M., Altmann D., Auffenberg J., et al. 2013, ArXiv e-prints  
 Kashfi T., Waxman E., 2005, Physical Review Letters, 95, 181101  
 Learned J. G., Pakvasa S., 1995, Astroparticle Physics, 3, 267  
 Liang E., Zhang B., Virgili F., Dai Z. G., 2007, The Astrophysical Journal, 662, 1111  
 Mena O., Mocioiu I., Razzaque S., 2007, Phys. Rev. D, 75, 063003  
 Mena O., Palomares-Ruiz S., Vincent A. C., 2014, ArXiv e-prints  
 Mészáros P., 2006, Reports on Progress in Physics, 69, 2259  
 Meszaros P., Rees M. J., 1994, MNRAS, 269, L41  
 Mészáros P., Waxman E., 2001, Phys. Rev. Lett., 87, 171102  
 Mizuta A., Ioka K., 2013, ApJ, 777, 162  
 Mohapatra R. N., Pal P. B., 2004, Massive neutrinos in physics and astrophysics  
 Murase K., Inoue Y., Dermer C. D., 2014, ArXiv e-prints  
 Murase K., Ioka K., 2013, Physical Review Letters, 111, 121102  
 Murase K., Kashiyama K., Mészáros P., 2013, Physical Review Letters, 111, 131102  
 Nötzold D., Raffelt G., 1988, Nuclear Physics B, 307, 924  
 Nunokawa H., Parke S., Valle J. W. F., 2008, Progress in Particle and Nuclear Physics, 60, 338  
 Osorio Oliveros A. F., Sahu S., Sanabria J. C., 2013, ArXiv e-prints  
 Paczynski B., Rhoads J. E., 1993, ApJ, 418, L5  
 Piran T., 2005, in de Gouveia dal Pino E. M., Lugones G., Lazarian A., eds, Magnetic Fields in the Universe: From Laboratory and Stars to Primordial Structures. Vol. 784 of American Institute of Physics Conference Series, Magnetic Fields in Gamma-Ray Bursts: A Short Overview. pp 164–174  
 Razzaque S., 2013, Phys. Rev. D, 88, 081302  
 Razzaque S., Mészáros P., Waxman E., 2004, Physical Review Letters, 93, 181101  
 Razzaque S., Smirnov A. Y., 2010, Journal of High Energy Physics, 3, 31  
 Rees M. J., Meszaros P., 1994, ApJ, 430, L93  
 Ruffert M., Janka H.-T., 1999, A&A, 344, 573  
 Sahu S., Fraija N., Keum Y.-Y., 2009a, Phys. Rev. D, 80, 033009  
 Sahu S., Fraija N., Keum Y.-Y., 2009b, J. Cosmology Astropart. Phys., 11, 24  
 Sahu S., Zhang B., 2010, Research in Astronomy and Astrophysics, 10, 943  
 Schwinger J., 1951, Physical Review, 82, 664  
 Shigeyama T., Nomoto K., 1990, ApJ, 360, 242  
 Soderberg et al. 2006, Nature, 442, 1014  
 Soderberg A. M., et al. 2010, Nature, 463, 513  
 Taboada I., 2010, Phys. Rev. D, 81, 083011  
 Volkas R. R., Wong Y. Y., 2000, Astroparticle Physics, 13, 21  
 Waxman E., 2013, ArXiv e-prints  
 Wendell R., et al. 2010, Phys. Rev. D, 81, 092004  
 Wolfenstein L., 1978a, Phys. Rev. D, 17, 2369  
 Wolfenstein L., 1978b, Phys. Rev. D, 17, 2369  
 Woosley S. E., Langer N., Weaver T. A., 1993, ApJ, 411, 823  
 Zeitnitz B., 1994, Progress in Particle and Nuclear Physics, 32, 351  
 Zhang B., Mészáros P., 2004, International Journal of Modern Physics A, 19, 2385

## APPENDIX A: EFFECTIVE POTENTIAL

The functions of the neutrino effective potential at moderate magnetic field limit are

$$\begin{aligned}
 F_m &= \left(1 + 2\frac{E_\nu^2}{m_W^2}\right) K_1(\sigma_l) + 2 \sum_{n=1}^{\infty} \lambda_n \left(1 + \frac{E_\nu^2}{m_W^2}\right) K_1(\sigma_l \lambda_n) \\
 G_m &= \left(1 - 2\frac{E_\nu^2}{m_W^2}\right) K_1(\sigma_l) - 2 \sum_{n=1}^{\infty} \lambda_n \frac{E_\nu^2}{m_W^2} K_1(\sigma_l \lambda_n) \\
 J_m &= \frac{3}{4} K_0(\sigma_l) + \frac{K_1(\sigma_l)}{\sigma_l} + \sum_{n=1}^{\infty} \lambda_n^2 \left[ K_0(\sigma_l \lambda) + \frac{K_1(\sigma_l \lambda)}{\sigma_l \lambda} \right. \\
 &\quad \left. - \frac{K_0(\sigma_l \lambda)}{2\lambda_n^2} \right] \\
 H_m &= \frac{K_1(\sigma_l)}{\sigma_l} + \sum_{n=1}^{\infty} \lambda_n^2 \left[ \frac{K_1(\sigma_l \lambda)}{\sigma_l \lambda} - \frac{K_0(\sigma_l \lambda)}{2\lambda_n^2} \right] \quad (A1)
 \end{aligned}$$

and at weak magnetic field limit are

$$\begin{aligned}
 F_w &= \left(2 + 2\frac{E_\nu^2}{m_W^2}\right) \left(\frac{K_0(\sigma_l)}{\sigma_l} + 2\frac{K_1(\sigma_l)}{\sigma_l^2}\right) \frac{B_c}{B} - K_1(\sigma_l) \\
 G_w &= K_1(\sigma_l) - \frac{2B_c}{B} \frac{E_\nu^2}{m_W^2} \left(\frac{K_0(\sigma_l)}{\sigma_l} + 2\frac{K_1(\sigma_l)}{\sigma_l^2}\right) \\
 J_w &= \left(\frac{1}{2} + \frac{3B_c}{B\sigma_l^2}\right) K_0(\sigma_l) + \frac{B_c}{B} \left(1 + \frac{6}{\sigma_l^2}\right) \frac{K_1(\sigma_l)}{\sigma_l} \\
 H_w &= \left(\frac{1}{2} + \frac{B_c}{B\sigma_l^2}\right) K_0(\sigma_l) + \frac{B_c}{B} \left(\frac{2}{\sigma_l^2} - \frac{1}{2}\right) \frac{K_1(\sigma_l)}{\sigma_l} \quad (A2)
 \end{aligned}$$

where  $\lambda_n^2 = 1 + 2nB/B_c$ ,  $K_i$  is the modified Bessel function of integral order  $i$ ,  $\alpha_l = \beta\mu(l+1)$  and  $\sigma_l = \beta m_e(l+1)$ .

## APPENDIX B: PROBABILITIES

The flavor ratio at the internal shocks and the envelope of the star are

$$\begin{pmatrix} \nu_e \\ \nu_\mu \\ \nu_\tau \end{pmatrix}_{is} = \begin{pmatrix} P_{ee,is} & P_{em,is} & P_{et,is} \\ P_{me,is} & P_{mm,is} & P_{mt,is} \\ P_{te,is} & P_{tm,is} & P_{tt,is} \end{pmatrix} \begin{pmatrix} \nu_e \\ \nu_\mu \\ \nu_\tau \end{pmatrix}_c \quad (B1)$$

and

$$\begin{pmatrix} \nu_e \\ \nu_\mu \\ \nu_\tau \end{pmatrix}_{ss} = \begin{pmatrix} P_{ee,ss} & P_{em,ss} & P_{et,ss} \\ P_{me,ss} & P_{mm,ss} & P_{mt,ss} \\ P_{te,ss} & P_{tm,ss} & P_{tt,ss} \end{pmatrix} \begin{pmatrix} \nu_e \\ \nu_\mu \\ \nu_\tau \end{pmatrix}_{is} \quad (B2)$$

respectively Here  $ss$  and  $is$  are the envelope of star and internal shocks, respectively. The different neutrino probabilities can be written as (Gonzalez-Garcia & Nir 2003; Gonzalez-Garcia & Maltoni 2008)

$$\begin{aligned}
 P_{ee} &= 1 - 4s_{13,m}^2 c_{13,m}^2 S_{31} \\
 P_{\mu\mu} &= 1 - 4s_{13,m}^2 c_{13,m}^2 s_{23}^4 S_{31} - 4s_{13,m}^2 s_{23}^2 c_{23}^2 S_{21} - 4c_{13,m}^2 s_{23}^2 c_{23}^2 S_{32} \\
 P_{\tau\tau} &= 1 - 4s_{13,m}^2 c_{13,m}^2 c_{23}^4 S_{31} - 4s_{13,m}^2 s_{23}^2 c_{23}^2 S_{21} - 4c_{13,m}^2 s_{23}^2 c_{23}^2 S_{32} \\
 P_{e\mu} &= 4s_{13,m}^2 c_{13,m}^2 s_{23}^2 S_{31} \\
 P_{e\tau} &= 4s_{13,m}^2 c_{13,m}^2 c_{23}^2 S_{31} \\
 P_{\mu\tau} &= -4s_{13,m}^2 c_{13,m}^2 s_{23}^2 c_{23}^2 S_{31} + 4s_{13,m}^2 s_{23}^2 c_{23}^2 S_{21} + 4c_{13,m}^2 s_{23}^2 c_{23}^2 S_{32} \quad (B3)
 \end{aligned}$$

where

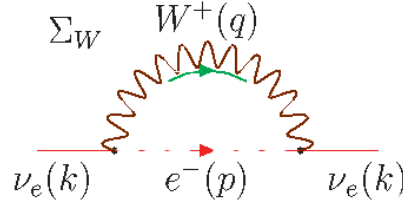


**Figure 1.** W-exchange diagram of one-loop contribution to the neutrino self-energy in a magnetized medium. The dashed line represents the electron propagator  $e^-(p)$ , the solid line corresponds to the electron neutrino propagator  $\nu_e(k)$  and the wiggly line is the W-boson propagator  $W^+(q)$ .

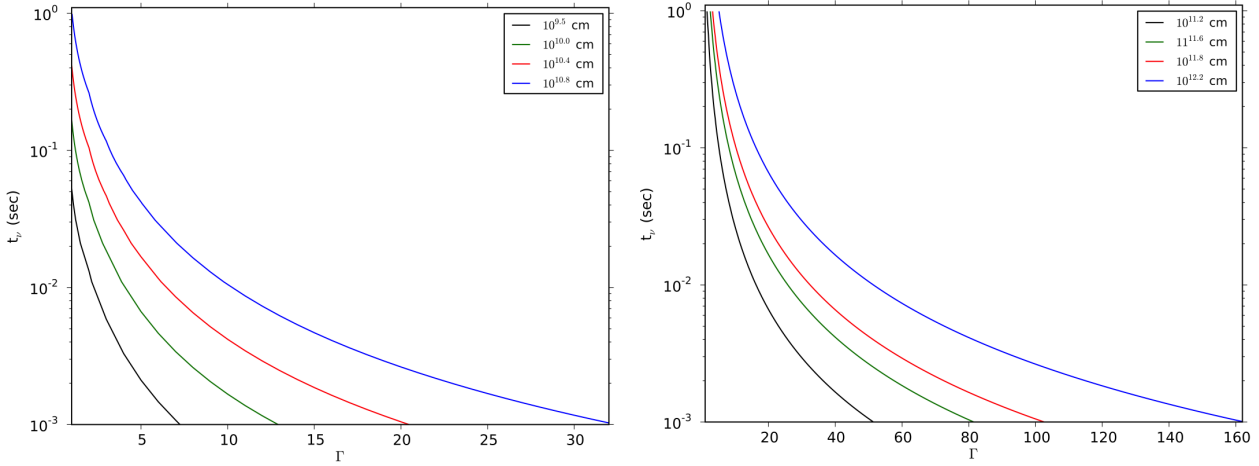


**Figure 2.** Contour lines of variability time scale ( $t_\nu$ ) and bulk Lorentz factor ( $\Gamma$ ) as a function of the distance of the internal shocks ( $r_j$ ) for which these shocks take place inside the progenitors. We have considered progenitors such as WR (left-hand figure) and BSG (right-hand figure) stars.

$$\sin 2\theta_{13,m} = \frac{\sin 2\theta_{13}}{\sqrt{(\cos 2\theta_{13} - 2E_\nu V_{eff,k}/\delta m_{32}^2)^2 + (\sin 2\theta_{13})^2}}, \quad (\text{B4})$$

and

$$S_{ij} = \sin^2 \left( \frac{\Delta\mu_{ij}^2 L}{4E_\nu} \right). \quad (\text{B5})$$

Here  $\Delta\mu_{ij}^2$  are given by

$$\begin{aligned} \Delta\mu_{21}^2 &= \frac{\Delta m_{32}^2}{2} \left( \frac{\sin 2\theta_{13}}{\sin 2\theta_{13,m}} - 1 \right) - E_\nu V_{eff,k}, \\ \Delta\mu_{32}^2 &= \frac{\Delta m_{32}^2}{2} \left( \frac{\sin 2\theta_{13}}{\sin 2\theta_{13,m}} + 1 \right) + E_\nu V_{eff,k}, \\ \Delta\mu_{31}^2 &= \Delta m_{32}^2 \frac{\sin 2\theta_{13}}{\sin 2\theta_{13,m}}, \end{aligned} \quad (\text{B6})$$

where

$$\begin{aligned} \sin^2 \theta_{13,m} &= \frac{1}{2} \left( 1 - \sqrt{1 - \sin^2 2\theta_{13,m}} \right), \\ \cos^2 \theta_{13,m} &= \frac{1}{2} \left( 1 + \sqrt{1 - \sin^2 2\theta_{13,m}} \right). \end{aligned} \quad (\text{B7})$$

where the neutrino effective potentials  $V_{eff,k}$  are given in section 3. In vacuum, the flavor ratio (between the surface of the star and the Earth) is affected by the oscillation probabilities (Giunti & Chung

2007; Bahcall 1989)

$$\begin{aligned} P_{\nu_\alpha \rightarrow \nu_\beta} &= |\langle \nu_\beta(t) | \nu_\alpha(t=0) \rangle| \\ &= \delta_{\alpha\beta} - 4 \sum_{j>i} U_{\alpha i} U_{\beta i} U_{\alpha j} U_{\beta j} \sin^2 \left( \frac{\delta m_{ij}^2 L}{4E_\nu} \right) \end{aligned} \quad (\text{B8})$$

where the neutrino mixing matrix  $U_{ij}$  is given by Gonzalez-Garcia & Nir (2003); Akhmedov et al. (2004); Gonzalez-Garcia (2011)

$$U = \begin{pmatrix} c_{13}c_{12} & s_{12}c_{13} & s_{13} \\ -s_{12}c_{23} - s_{23}s_{13}c_{12} & c_{23}c_{12} - s_{23}s_{13}s_{12} & s_{23}c_{13} \\ s_{23}s_{12} - s_{13}c_{23}c_{12} & -s_{23}c_{12} - s_{13}s_{12}c_{23} & c_{23}c_{13} \end{pmatrix}, \quad (\text{B9})$$

Here  $s_{ij} = \sin \theta_{ij}$  and  $c_{ij} = \cos \theta_{ij}$  and we have taken the Dirac phase  $\delta = 0$ . Taking into account the effect of internal shocks, envelope of star and the vacuum, the probabilities are given by

$$\begin{aligned} P_{11}^* &= 0.82 P_{11} + 0.55 P_{21} + 0.19 P_{31} \\ P_{12}^* &= 0.82 P_{12} + 0.55 P_{22} + 0.19 P_{32} \\ P_{13}^* &= 0.82 P_{13} + 0.55 P_{23} + 0.19 P_{33} \\ P_{21}^* &= -0.51 P_{11} + 0.51 P_{21} + 0.69 P_{31} \\ P_{22}^* &= -0.51 P_{12} + 0.51 P_{22} + 0.69 P_{32} \\ P_{23}^* &= -0.51 P_{13} + 0.51 P_{23} + 0.69 P_{33} \\ P_{31}^* &= 0.28 P_{11} - 0.66 P_{31} + 0.69 P_{31} \\ P_{32}^* &= 0.28 P_{12} - 0.66 P_{22} + 0.69 P_{32} \\ P_{33}^* &= 0.28 P_{13} - 0.66 P_{23} + 0.69 P_{33} \end{aligned} \quad (\text{B10})$$



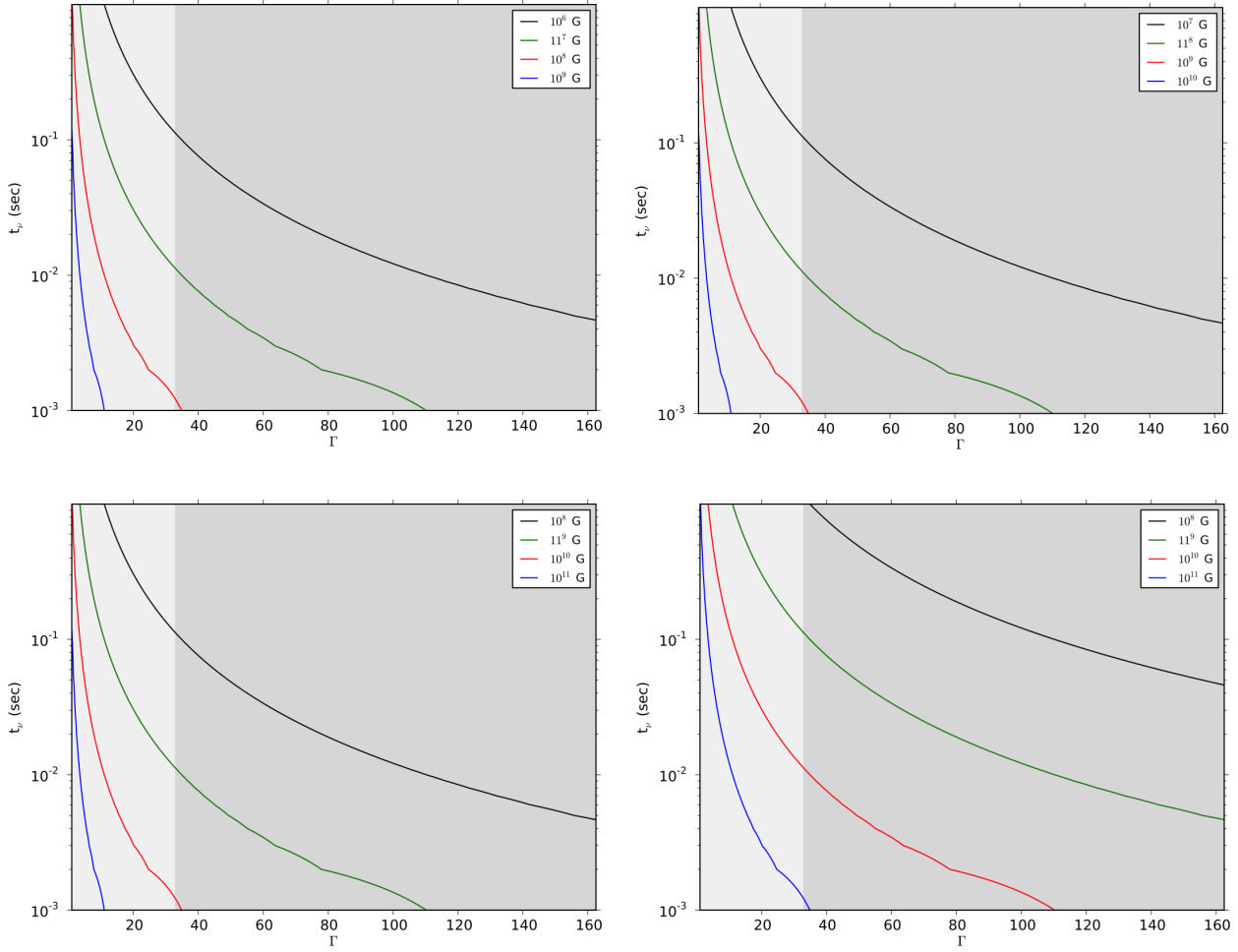


**Figure 3.** Contour lines of variability time scale ( $t_\nu$ ) and bulk Lorentz factor ( $\Gamma$ ) as a function of magnetic field ( $B'$ ) generated at internal shocks (eq. 1) inside a WR (light gray background) and a BSG (dark gray background). In the left-hand figure above (below) a luminosity of  $10^{46}$  ( $10^{50}$ ) erg/s was used, whereas in the right-hand figure above (below) it corresponds to a luminosity of  $10^{48}$  ( $10^{52}$ ) erg/s.

where

$$\begin{aligned}
 P_{11} &= P_{ee,ss}P_{ee,is} + P_{e\mu,ss}P_{\mu e,is} + P_{e\tau,ss}P_{\tau e,is} \\
 P_{12} &= P_{ee,ss}P_{e\mu,is} + P_{e\mu,ss}P_{\mu\mu,is} + P_{e\tau,ss}P_{\tau\mu,is} \\
 P_{13} &= P_{ee,ss}P_{e\tau,is} + P_{e\mu,ss}P_{\mu\tau,is} + P_{e\tau,ss}P_{\tau\tau,is} \\
 P_{21} &= P_{e\mu,ss}P_{ee,is} + P_{\mu\mu,ss}P_{\mu e,is} + P_{m\tau,ss}P_{\tau e,is} \\
 P_{22} &= P_{\mu e,ss}P_{e\mu,is} + P_{\mu\mu,ss}P_{\mu\mu,is} + P_{m\tau,ss}P_{\tau\mu,is} \\
 P_{23} &= P_{\mu e,ss}P_{e\tau,is} + P_{\mu\mu,ss}P_{\mu\tau,is} + P_{m\tau,ss}P_{\tau\tau,is} \\
 P_{31} &= P_{e\tau,ss}P_{ee,is} + P_{\tau\mu,ss}P_{\mu e,is} + P_{\tau\tau,ss}P_{\tau e,is} \\
 P_{32} &= P_{\tau e,ss}P_{e\mu,is} + P_{\tau\mu,ss}P_{\mu\mu,is} + P_{\tau\tau,ss}P_{\tau\mu,is} \\
 P_{33} &= P_{\tau e,ss}P_{e\tau,is} + P_{\tau\mu,ss}P_{\mu\tau,is} + P_{\tau\tau,ss}P_{\tau\tau,is} \quad (B11)
 \end{aligned}$$

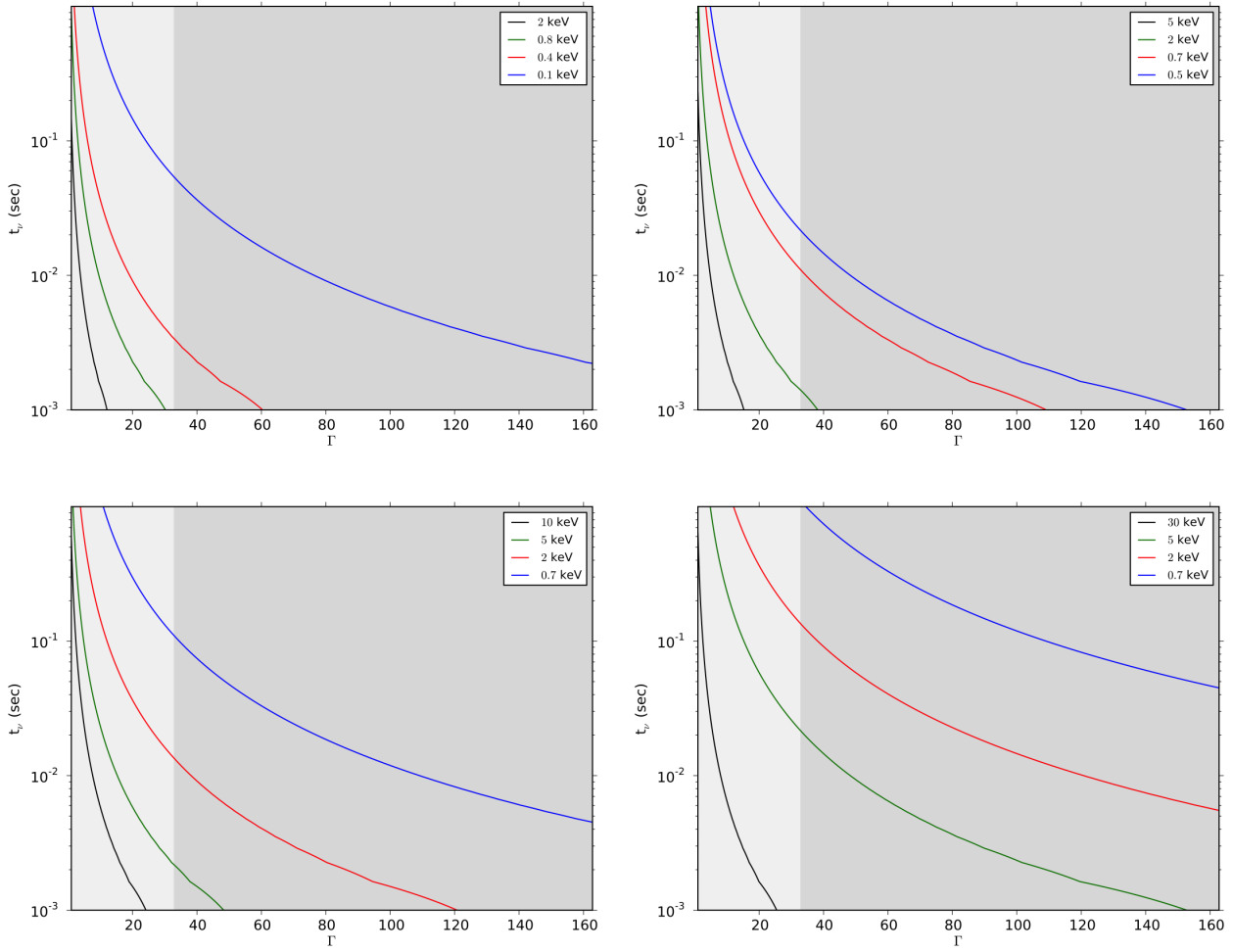


**Figure 4.** Contour lines of variability time scale ( $t_\nu$ ) and bulk Lorentz factor ( $\Gamma$ ) as a function of synchrotron photons created in internal shocks and thermalized to a black body temperature ( $T'_j$ ) (eq. 2). Once again we consider a WR (light gray background) and a BSG (dark gray background). In the left-hand figure above (below) a luminosity of  $10^{46}$  ( $10^{50}$ ) erg/s was used whereas in the right-hand figure above (below) it corresponds to a luminosity of  $10^{48}$  ( $10^{52}$ ) erg/s

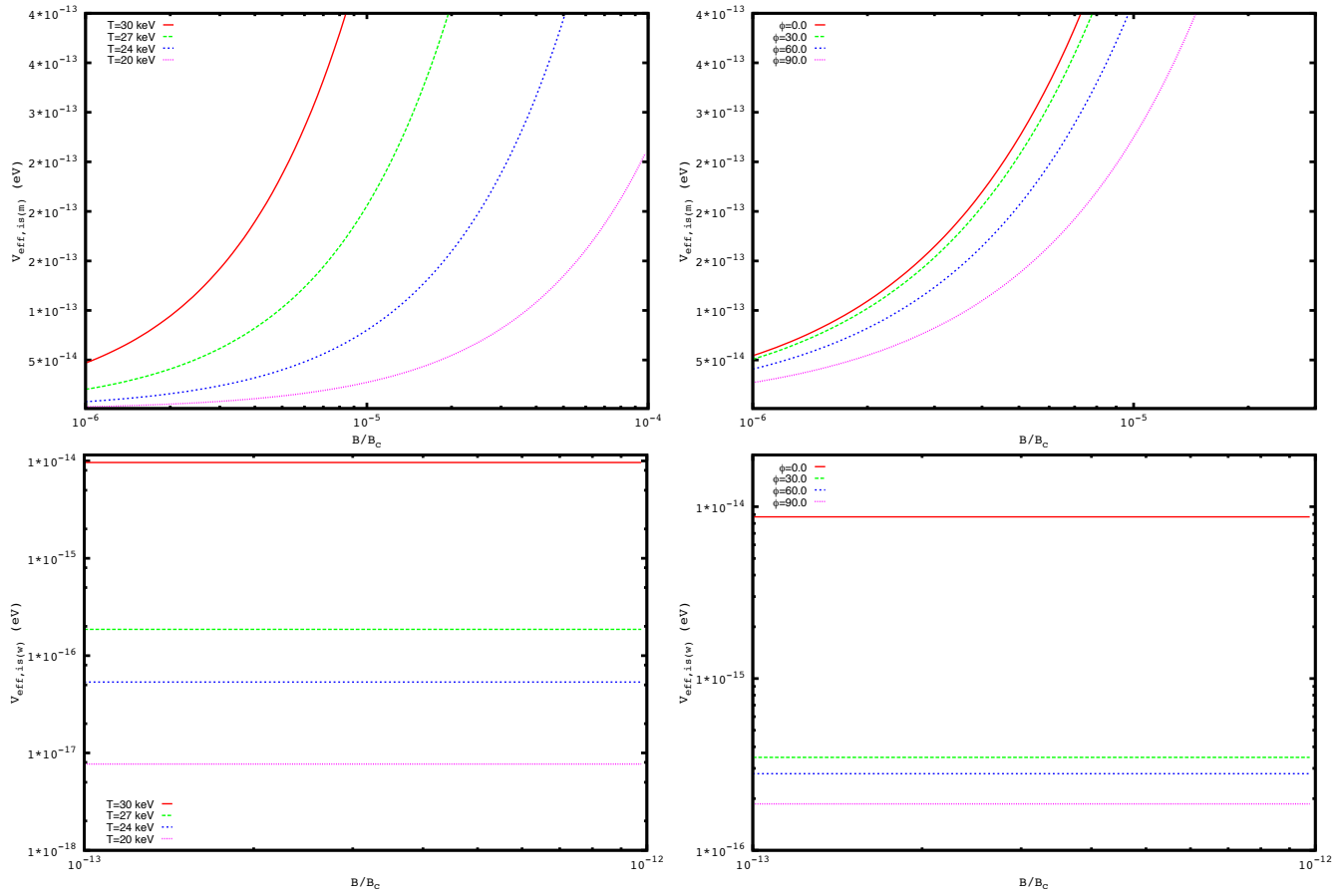


**Figure 5.** Neutrino effective potentials at moderate (top) and weak (bottom) limits are plotted as a function of magnetic field for temperatures at keV energies (left) and different angles between the direction of neutrino propagation and magnetic field (right).

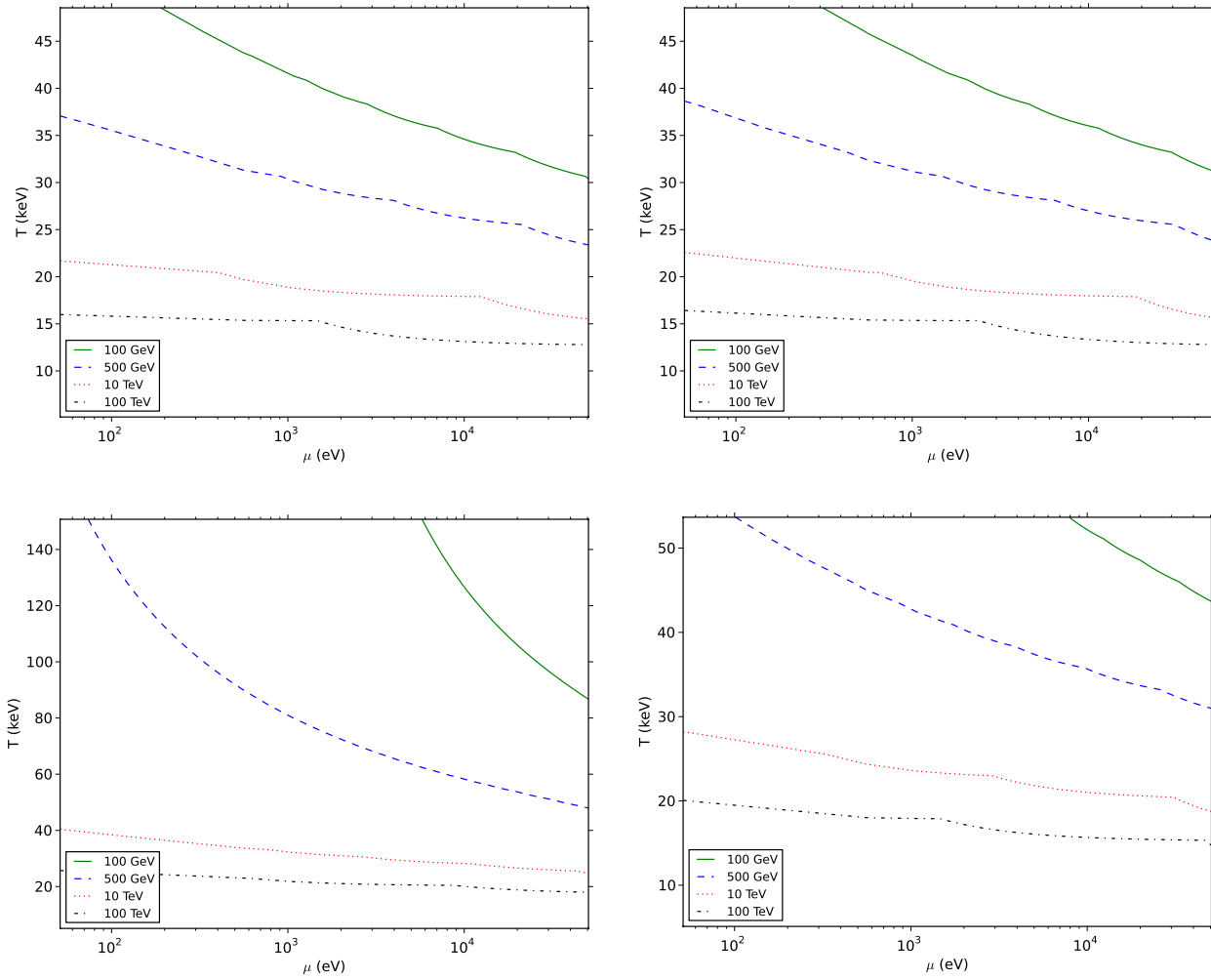


**Figure 6.** Contour lines of temperature and chemical potential as a function of neutrino energy for which the resonance condition is satisfied. We have used the neutrino effective potential at the moderate limit (eq. 19) and the best-fit values of the two-neutrino mixing (solar, top left; atmospheric, top right; and accelerator, bottom left) and three-neutrino mixing (bottom right).

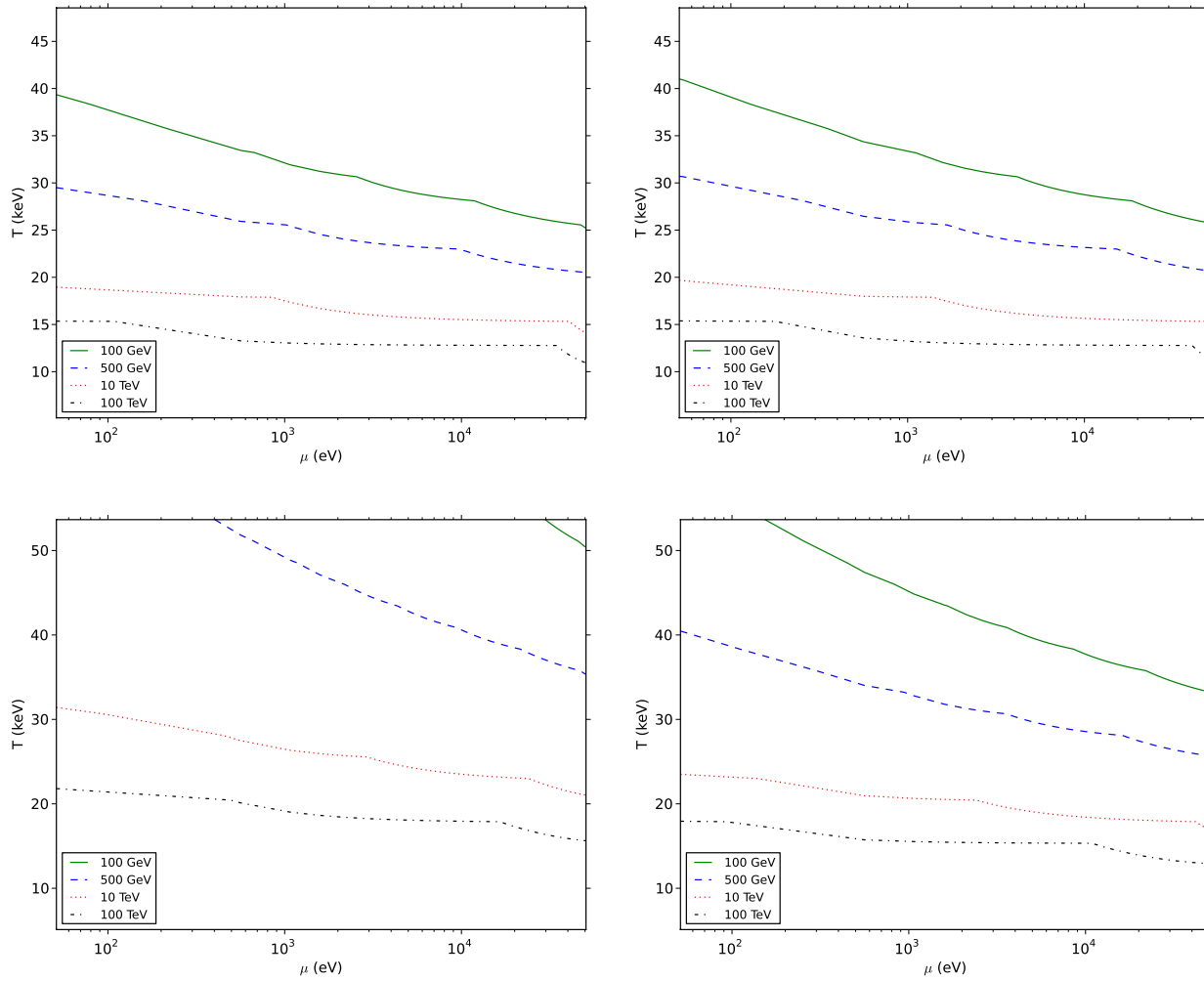


**Figure 7.** Contour lines of temperature and chemical potential as a function of neutrino energy for which the resonance condition is satisfied. We have used the neutrino effective potential at the weak limit (eq. 20) and the best-fit values of the two-neutrino mixing (solar, top left; atmospheric, top right; and accelerator, bottom left) and three-neutrino mixing (bottom right).

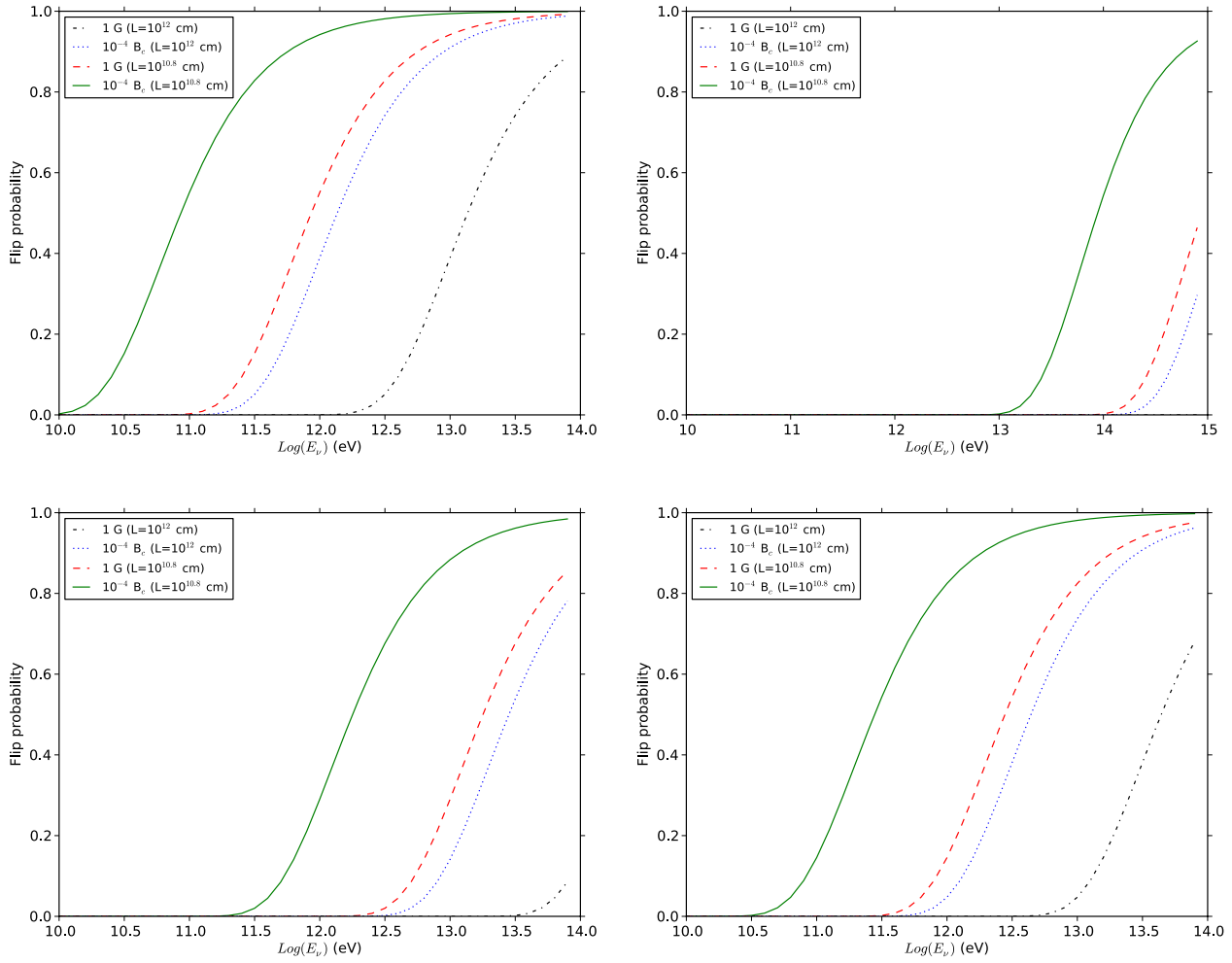


**Figure 8.** The flip probability is plotted as a function of neutrino energy for a strength of magnetic field in the moderate ( $B=10^{-4} B_c$ ) and weak ( $B=1$  G) regime and at a distance of  $10^{10.8}$  cm and  $10^{12}$  cm. We have used the best-fit values of the two-neutrino mixing (solar, top left; atmospheric, top right; and accelerator, bottom left) and three-neutrino mixing (bottom right).

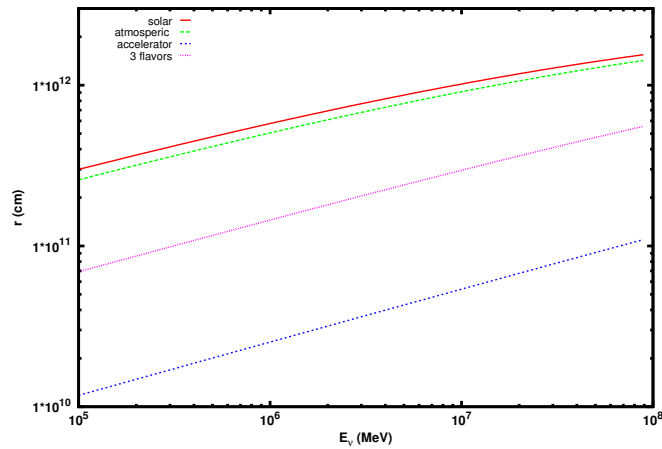


**Figure 9.** Contour lines of distance and neutrino energy as a function of neutrino oscillation parameters for which the resonance condition is satisfied. We have used the neutrino effective potential generated by the envelope of star (eq. 23) and the best parameters of neutrino oscillation for solar, atmospheric, accelerator and three flavors.

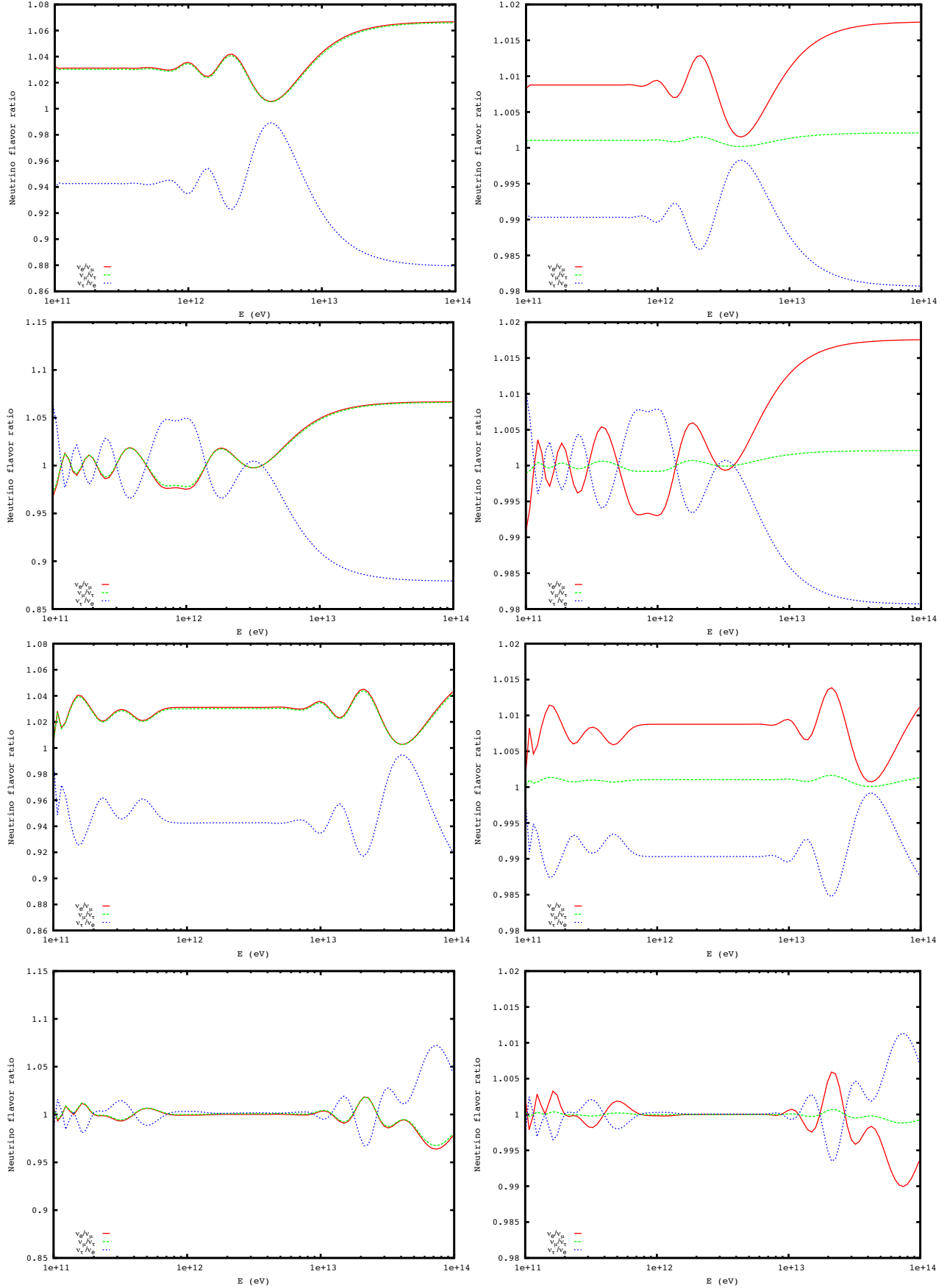


**Figure 10.** Neutrino flavor ratio expected on Earth as a function of neutrino energy when these are created on the surface of a WR (at  $10^{11}$  and  $10^{10.8}$  cm for the upper and second panels, respectively) and a BSG (at  $10^{12.3}$  and  $10^{12}$  cm for the third and bottom panels, respectively). We have used the neutrino effective potential at the moderate (second and bottom panels) and weak (upper and third panels) field limit for  $\theta_{13}=11^\circ$  (left) and  $\theta_{13} = 2^\circ$ . (right)

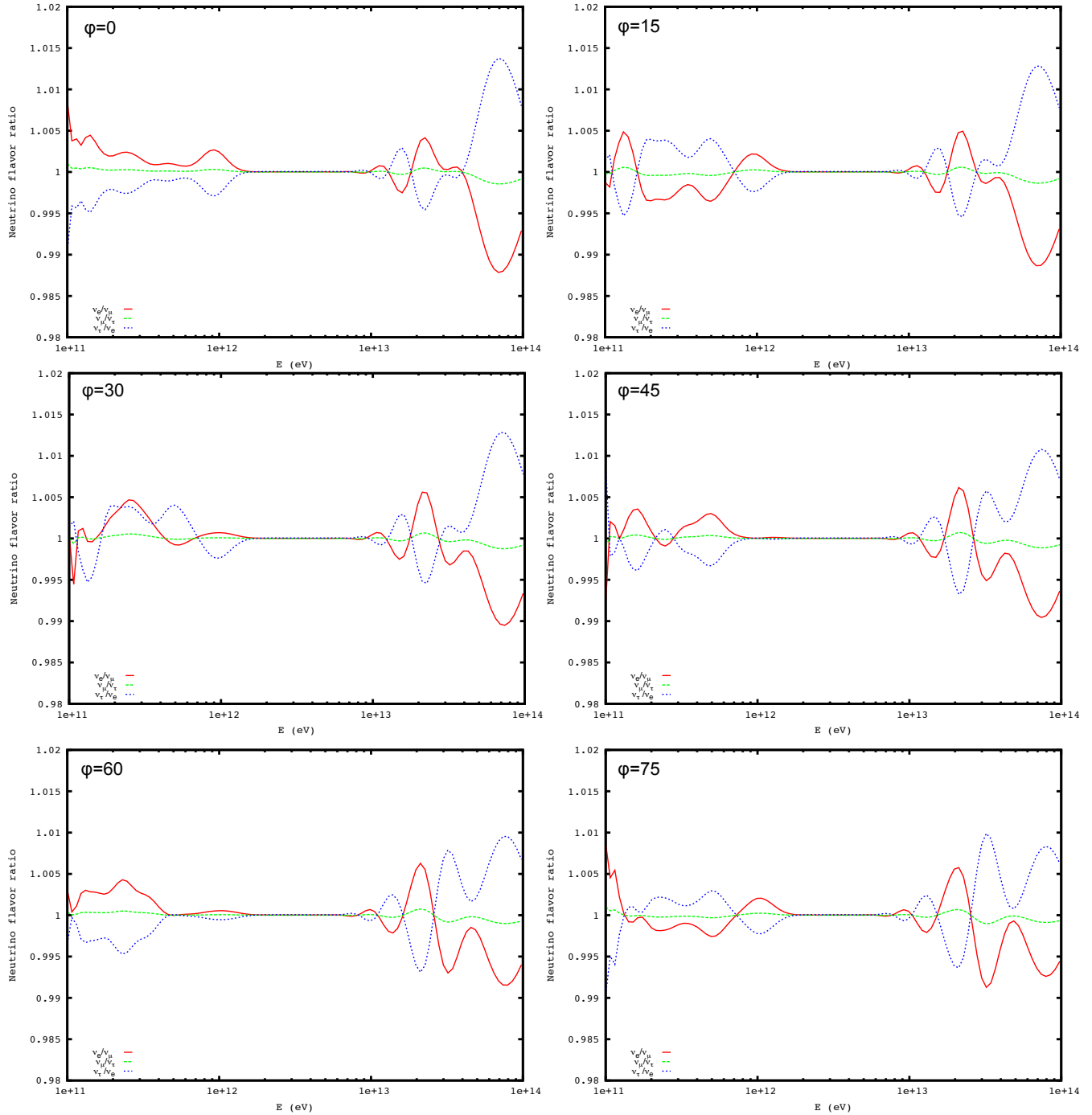


**Figure 11.** Neutrino flavor ratio expected on Earth as a function of neutrino energy when these are created on the surface of a BSG. We have considered that internal shocks take place at  $r_j = 10^{12}$  cm with a physical width  $\Delta r_j = 2 \times 10^{11}$  cm and the magnetic field is oriented to different angles  $0^\circ \leq \varphi \leq 75^\circ$  concerning to neutrino direction. We have used the neutrino effective potential at the moderate-field limit (eq. 19) and  $\theta_{13} = 2^\circ$ .



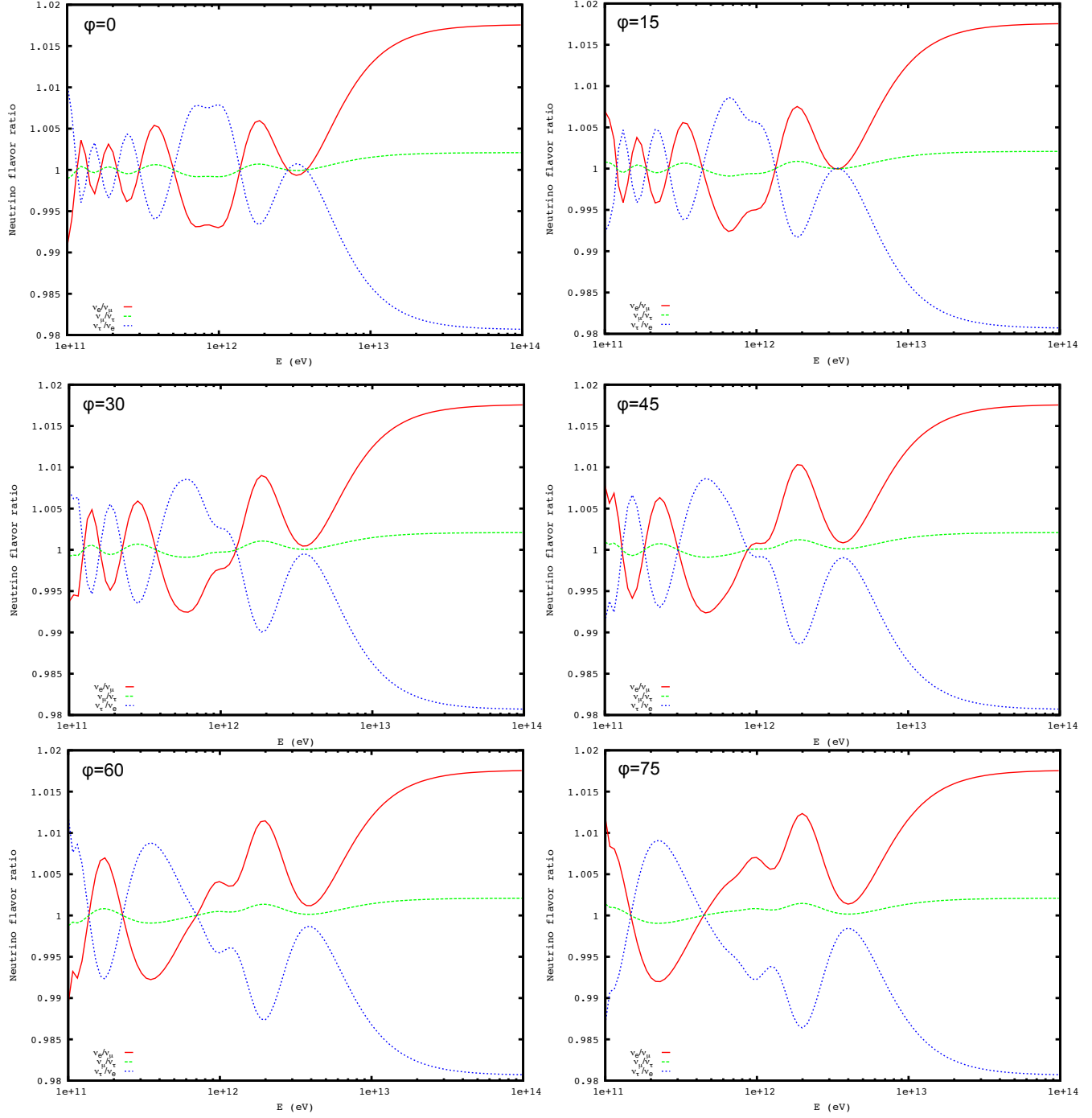


**Figure 12.** Neutrino flavor ratio expected on Earth as a function of neutrino energy when these are created on the surface of a BSG. We have considered that internal shocks take place at  $r_j = 10^{12}$  cm with a physical width  $\Delta r_j = 2 \times 10^{11}$  cm and the magnetic field is oriented to different angles  $0^\circ \leq \varphi \leq 75^\circ$  concerning neutrino direction. We have used the neutrino effective potential at the moderate-field limit (eq. 20) and  $\theta_{13} = 2^\circ$ .